International Journal of Thermofluids 22 (2024) 100667

Contents lists available at ScienceDirect

International Journal of Thermofluids

journal homepage: www.sciencedirect.com/journal/international-journal-of-thermofluids

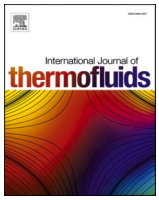

The influence of residual gas on ozone-assisted combustion in an HCCI reciprocating engine

Marco D'Amato [a,*], Vinicio Magi [a,b], Annarita Viggiano [a]

[a] School of Engineering, University of Basilicata, 85100 Potenza, Italy
[b] Department of Mechanical Engineering, San Diego State University, San Diego, CA 92182, USA

ARTICLE INFO

Keywords:
HCCI engine
Ozone assisted combustion
Residual gases
Iso-octane
Performance
Emissions

ABSTRACT

This work is an investigation on the influence of both residual gas and ozone on the combustion process in an HCCI engine fuelled with iso-octane/air/ozone mixtures and on how ozone reacts with residual gases. It is well known that ozone releases oxygen atoms mainly through the $O_3 + M \rightleftarrows O_2 + O + M$ reaction and this may lead to an improvement of the engine combustion. Nevertheless, the chemical interaction between ozone and the species in the residual gas has not yet been investigated in the literature. CFD simulations of a closed-valve engine cycle have been carried out by using an axisymmetric domain. The model has been validated against experimental data and a parametric analysis has been carried out to assess different compositions and amounts of residual gases on the engine performance. The results show that during compression ozone enables Low-Temperature Combustion, with a small amount of heat released before the occurrence of auto-ignition. The combustion is faster and advanced with a reduction of UHCs and an increase of NO_x. The results show that the influence of ozone is more effective as the mass of residual gases increases. With an ozone concentration of 35 ppm at IVC the gross work per cycle increases by 2.52 %, 3.58 % and 5.7 %, compared to the case without ozone, with 0 %, 5 % and 10 % by mass of residual gases, respectively. It can be concluded that ozone is more beneficial for cases where combustion is slower due to the higher amount of residual gases.

1. Introduction

In the last decades, world energy consumption has continued to grow significantly, from about 88,000 TWh in 1980 to about 177,000 TWh in 2021, more than doubling over 41 years [1,2]. Despite producing more and more energy from renewable resources every year, the global energy mix is still dominated by fossil fuels, whose consumption is globally increasing [1]. In the International Energy Outlook 2021 (IEO2021) [2], the U.S. Energy Information Administration stated that global energy consumption will increase by almost 50 % over the next 30 years, and the majority of this increase will be driven by non-OECD (Organization for Economic Cooperation and Development) countries, mainly due to the continuous population growth and the development needs of weak and less technological countries. Renewable energy resources, such as solar and wind energy, have strong fluctuations and are not always available and enough to meet energy demand. Therefore, combustion still plays a fundamental role in the today's society, both for transportation and for energy production. The increase in global energy demand, however, conflicts with the need to reduce polluting emissions in order to safeguard the environment and human health. About three-quarters of global Greenhouse Gas (GHG) emissions come from the energy sector (about 73.2 %), while the transport sector accounts for a contribution of about 16.2 %. Road transport accounts for about three-quarters of transport emissions; most of this comes from passenger vehicles (cars and buses), which contribute 45.1 %, and the other 29.4 % comes from freight trucks [3,4].

Considering both the energy and the climate context, there is a need to develop efficient strategies and technologies for Internal Combustion Engines (ICEs), in terms of both performance and reduction of pollutant emissions. Several new combustion strategies aim to combine the advantages of Spark Ignition (SI) engines with those of Compression Ignition (CI) engines, while reducing the negative aspects of both technologies. In most cases, these unconventional engines are based on Low Temperature Combustion (LTC) strategies [5–7], such as the Homogeneous Charge Compression Ignition (HCCI) combustion engine, which are characterized by low emissions, such as SI engines, and high efficiency, such as CI engines. Specifically, HCCI engines are characterized by very fast combustion of highly diluted fuel vapor and air. The

* Corresponding author.
E-mail address: marco.damato@unibas.it (M. D'Amato).

https://doi.org/10.1016/j.ijft.2024.100667

Available online 18 April 2024

mixture of fuel and air is compressed until near-simultaneous auto--ignition occurs at several locations in the combustion chamber. The use of a highly diluted mixture limits soot production and reduces the risk of detonation. Moreover, thermal NO_x formation decreases significantly, since the average combustion temperature is relatively low [7–9].

In HCCI engines auto-ignition and the whole combustion process are governed by a complicated chemical kinetics, so the proper control of chemistry is the crucial aspect of this type of engine. Other critical issues concern with the i) imperfect charge homogeneity; ii) emissions of unburned hydrocarbons (UHCs) and *CO* due to the need to operate at very low equivalence ratios such that incomplete combustion may occur; iii) high pressure rise rate due to the quasi-simultaneous occurrence of many ignition kernels; iiii) high cycle-to-cycle variability and narrow engine operating range. In order to overcome such challenges, many factors [10–12] have been investigated: equivalence ratio; composition and temperature of the charge [13]; the shape of the combustion chamber, which affects turbulence and combustion [14–16]; wall heat transfer; lubricating oil effect [17]; EGR [18,19]; the use of oxidising species, such as O_3 or NO_x [20–23].

As for the latter issue, many studies in recent decades have dealt with the properties of ozone and its influence on combustion systems [24]. There are several features of ozone that are interesting in the combustion process. One of those is its relatively long lifetime (about 25 h at room conditions and zero humidity) [25]. Thus, ozone can be available in the combustion chamber to promote fuel oxidation. Another relevant aspect of ozone is its efficient and economical production even under high-pressure conditions. These conditions are typical of most combustion devices. Studies conducted on ozone assisted combustion have covered several aspects such as: mixture ignition, flame propagation speed, flame structure and stability. The benefits of using ozone in combustion systems are mainly due to the atomic oxygen available by the ozone decomposition reaction, i.e. $O_3 + M \rightleftarrows O_2 + O + M$. Nomaguchi and Koda [26] measured the burning velocity of CH_4/Air mixture at room and stoichiometric conditions. The results showed that, by adding 5000 ppm of ozone to the mixture, the burn rate increases by 5 %. Similar results were also obtained by Halter et al. [27]. Ombrello et al. [28] investigated the thermal and kinetic effects of O_3 on flame propagation by using $C_3H_8/O_2/N_2$ laminar lifted flames. They observed an acceleration of chemical kinetics with ozone by comparing flame stabilization locations for cases with and without O_3. The IDT of a $CH_4/O_2/O_3/Ar$ mixture was studied by Xie et al. [29] using a Rapid Compression Machine (RCM), thus showing that IDT decreases with ozone addition. Similar results were also obtained by D'Amato et al. [30] for isooctane/O_3/air mixtures. Gao et al. [31] examined the effect of ozone on methane, propane and ethylene, finding that the laminar flame speed at room conditions increased for alkanes and decreased for ethylene, due to ozonolysis reactions. Vu et al. [32] carried out experiments with CH_4/air and C_3H_8/air mixtures, finding that ozone addition was able to stabilize an initially unstable flame, due to the increase in the laminar flame speed. Similar results were also obtained by Zhang et al. [33]. They found that the flammability limits of syngas were extended with ozone addition. Khan et al. [34] investigated the effects of O_3, *H, CO* and EGR addition to Haltermann gasoline by evaluating laminar and turbulent flame speeds using spherically propagating premixed flames in a constant volume combustion vessel. The authors found that the increase of the initial temperature and pressure of the mixture resulted in a significant increase in the laminar flame speed. Similar results were also obtained by D'Amato et al. [35,36], who conducted a numerical investigation on the laminar flame speed of iso-octane/air and methane/air mixtures. With iso-octane, ozone can generate a cool flame [35], thus increasing the laminar flame speed due to the different reaction paths. Recently, the influence of ozone on flame ignition and propagation, detonation and explosion limits for H_2/O_2 mixtures has been investigated in [37–40]. The main conclusions are that ozone increases flame speed and influences both reactions and preferential diffusion, mainly due to the reaction with H, i.e. $H + O_3 \rightleftarrows O_2 + OH$.

Since ozone influences ignition timing and flame acceleration and stabilization, various ICEs parameters may be influenced, such as ignition timing, heat release rate, operating range, pollutant emissions. Nishida and Tachibana [41] investigated the use of ozone to control the auto-ignition timing in an HCCI engine by conducting both experimental and numerical analyzes. The results encouraged the use of ozone for this purpose, showing that it is a good practice to control the auto-ignition timing by varying the ozone concentration. Similar results were also obtained by Foucher et al. [20], who studied the influence of ozone in an n-heptane-fuelled HCCI engine and observed that the addition of 50 ppm of O_3 was able to advance ignition by about 15 CAD. Masurier et al. [42] showed that the addition of ozone allows controlling the combustion phasing and increasing the indicated mean effective pressure in HCCI engines fed with alcohol fuels. Yamada et al. [43] studied the use of different additives in a mixture with DME as fuel in an HCCI engine, finding that ozone, other than advancing the auto-ignition timing, reduced the ignition temperature of the cool flame. Masurier et al. [22] considered different Primary Reference Fuels (PRFs) to evaluate ozone effect on a single cylinder of an HCCI engine. The authors found that ozone promoted the formation of a cool flame and advanced the entire combustion process. Masurier et al. [23] evaluated the influence of ozone with *NO* and NO_2 as additives, finding that ozone was the species that most advanced and accelerated the combustion process. Pinazzi and Foucher [44,45] investigated the influence of ozone in an engine operating under Partially Premixed Compression Ignition (PPCI) mode with direct gasoline injection. The authors found that ozone had a greater impact on the engine performance if fuel injection was advanced. Seignour et al. [46] carried out experiments using an ultraviolet light absorption diagnostic to understand the influence of specific parameters and species on ozone decomposition in an HCCI engine. They found that iso-octane and water vapor had a greater effect on ozone decomposition. Seignour et al. [47] examined ozone-assisted combustion in an HCCI engine, comparing hydrogen and iso-octane as fuels. Analyzes were conducted on the influence of intake pressure, intake temperature and ozone on the combustion for both fuels. They found that ozone had the greatest impact, and it was also used to shift the combustion region of isooctane in order to make a valid comparison with hydrogen. Anaclerio et al. [48] conducted experiments to evaluate the effect of ozone in a gasoline SI engine. The results showed an advance and increase in the in-cylinder pressure peak with ozone addition, resulting in auto-ignition and knocking for high ozone concentrations in stoichiometric mixtures, whereas, under lean conditions, ozone increased flame stability and shortened combustion duration.

The aim of this work is to evaluate the combined effect of ozone and residual gases in an HCCI engine fuelled by isooctane. Pinazzi e Foucher [44,45] showed that, in a PCCI engine, ozone effect is limited by the presence of nitrogen oxides, due to direct reactions between O_3 and NO_x. Similar results were also obtained by Masurier et al. [23], who studied the performance of an HCCI engine with three different oxidizing chemical species (O_3, *NO* and NO_2) added to the mixture. The results showed that, by injecting only one species, ozone was the species that most advanced the auto-ignition. By adding nitrogen monoxide and ozone to the mixture, a combustion delay occurred, with a molar fraction of ozone less than that of *NO*. As the mass of ozone increases to a value comparable to that of *NO*, an advanced combustion process occurred once again. These results suggest that the beneficial effect of ozone could be altered by the presence of *NO*, due to imperfect cylinder flushing and/or exhaust gas recirculation. On the other hand, there are both numerical and experimental studies that investigated the influence of ozone in compression ignition engines with the addition of EGR [46, 49–51]. Seignour et al. [46] carried out experiments using an ultraviolet light absorption diagnostic to understand the influence of N_2, CH_4, CO_2 and H_2O on ozone decomposition in an HCCI engine. The results showed that CO_2 has no effect on the rate of ozone decomposition. Instead, nitrogen, methane and humidity have a great impact, reducing the time of ozone decomposition as the amount of nitrogen, methane or water

vapour increases. Similar analyzes were carried out by Song and Foucher [49] under engine relevant conditions in a rapid compression machine. The authors found that ozone decomposition is promoted by steam. Furthermore, the enhancement of ozone decomposition in the presence of methane is lower compared to that obtained with iso-octane. Sayssouk et al. [50] developed a 0-D model to predict the combustion parameters of an HCCI engine with the addition of different amounts of ozone and EGR. However, EGR consisted only of N_2 to obtain different degrees of dilution and not to investigate the chemical reactions between EGR and ozone. In actual engines, EGR consists of thermal active components, such as *CO* or UHCs, that can influence the combustion timing. Kobashi et al. [51] carried out experiments on a GCI engine with the addition of ozone by recirculating a certain amount of exhaust gas. However, the chemical interaction between ozone and other species in the chamber was not investigated. In this scenario, the objective of this work is to understand how ozone reacts in the presence of residual gases for an HCCI engine. To our knowledge, this issue has never been investigated from others. To this end, CFD simulations have been carried out by using the Eddy Dissipation Concept (EDC) combustion model, to accurately solve the chemical kinetics. Specifically, a typical composition of residual gases has been considered and a parametric analysis has been carried out by varying the mass of residual gas and ozone to study their chemical interactions during compression and to assess the influence of ozone on the performance of the engine.

This work is organized as follows: first, the mathematical model, with emphasis on the combustion model, the test case and numerical method are described; then, both the validation results, based on experimental data available in the scientific literature, and the influence of ozone and residual gases on engine performances are discussed; finally, conclusions are summarized.

2. The model

Simulations have been performed by employing a 2-D CFD model, which solves the Reynolds-Averaged Navier-Stokes (RANS) equations by using the RNG $k-\varepsilon$ turbulence model with standard wall functions. A multicomponent diffusion model has been employed to solve the transport equations for each chemical species [52]. The Ansys® Academic Research CFD package, Release 20.2, [53] has been used for the simulations.

The combustion model and the numerical setup are detailed in the following subsections.

2.1. The combustion model

The Eddy–Dissipation Concept (EDC) model, proposed by Magnussen [54] and revisited with minor modifications [55], has been used to simulate turbulent combustion. The model assumes that a reacting fluid can be divided into two parts: the small turbulent structures (fine-scales), where chemical reactions occur, and the non-reactive region (surrounding fluid mixture). The characteristic length and time of the fine-scales [54,56,57] can be related to the kinematic viscosity of the fluid, ν, the turbulent kinetic energy, k, and the dissipation rate of turbulent kinetic energy, ε. This is because turbulence causes the mixing of chemical species between the fine-scales and the surrounding fluid, and the energy cascade occurs up to the Kolmogorov scales.

The fine-scales are defined as:

$$\xi^* = C_\xi \left(\frac{\nu\varepsilon}{k^2}\right)^{\frac{1}{4}} \tag{1}$$

$$\tau^* = C_\tau \left(\frac{\nu}{\varepsilon}\right)^{\frac{1}{2}}, \tag{2}$$

where ξ^* and τ^* are the dimensionless length fraction and the characteristic time of the fine structures, respectively, and C_ξ and C_τ are model parameters.

To compute a generic flow property, $\overline{\phi}$, the following equation is used:

$$\overline{\phi} = \phi^\circ \left[1-(\xi^*)^3\right] + \phi^*(\xi^*)^3, \tag{3}$$

where ϕ° is the fine-scales property and ϕ^* is the value in the surroundings. Therefore, the mean reaction rate of the *i-th* chemical species, $\bar{R}_i$, is defined as:

$$\overline{R}_i = \frac{\overline{\rho}(\xi^*)^2}{\tau^*}(Y_i^\circ - Y_i^*) \tag{4}$$

where $\bar{\rho}$ is the mean density of the fluid, and Y_i° and Y_i^* are the i-th chemical species mass fractions of the surrounding and the fine structures, respectively. Using Eqs. (1)–(3), $\bar{R}_i$ can be written as:

$$\bar{R}_i = \frac{\bar{\rho}(\xi^*)^2}{\tau^*\left[1-(\xi^*)^3\right]}(\bar{Y}_i - Y_i^*) \tag{5}$$

In spite of the original version of the EDC model, where the fine-structures are modeled as perfectly stirred reactors (PSRs), the fine-structures are treated as plug flow reactors (PFRs). With such an assumption, the fine structures are solved for the fine-scale characteristic time with a drastic reduction of the computational time. Hence, the following equation is solved at each time-step and in each numerical cell by assuming constant gas pressure and enthalpy during the time-step integration:

$$\frac{dY_i^*}{dt} = \dot{\omega}_i, \tag{6}$$

where $\dot{\omega}_i$ is the instantaneous net chemical production/consumption rate. The term $\dot{\omega}_i$ is computed by assuming that each reaction rate satisfies the law of mass action with the forward rate coefficient, k_f, given by the Arrhenius equation:

$$k_f = AT^\beta e^{\frac{-E_a}{RT}}, \tag{7}$$

where A is the pre-exponential factor, β is the temperature exponent and E_a is the activation energy. Eq. (6) is integrated over τ^* by using initial conditions based on the fluid properties.

Finally, the mixture composition is computed by using the transport equation of each chemical species:

$$\frac{\partial}{\partial t}(\rho\overline{Y}_i) + \overrightarrow{\nabla}\cdot(\rho\overrightarrow{v}\overline{Y}_i) = -\overrightarrow{\nabla}\cdot\overrightarrow{J}_i + \overline{R}_i \tag{8}$$

where ρ and $\overrightarrow{v}$ stand for density and velocity, respectively, $\bar{Y}_i$ is the mean mass fraction of the i-th chemical species, and $\overrightarrow{J}_i$ is the diffusive mass flux of species i in the mixture.

In the original version of the EDC model, the constants C_ξ and C_τ are set in order to extend the validity range of the model and to achieve a good compromise between theoretical considerations and experimental data. Specifically, C_ξ and C_τ are equal to 2.1377 and 0.4082, respectively [56]. For certain combustion configurations, such values have been

Table 1
Reference engine specifications.

Bore	85 mm
Stroke	88 mm
Connecting rod	145 mm
Displaced volume	499 cc
Geometric compression ratio	16:1
Intake valve closure IVC	157 CAD BTDC
Exhaust valve opening EVO	140 CAD ATDC
Equivalence Ratio	0.3
Engine Speed	1500 rpm
Fuel	Iso-octane

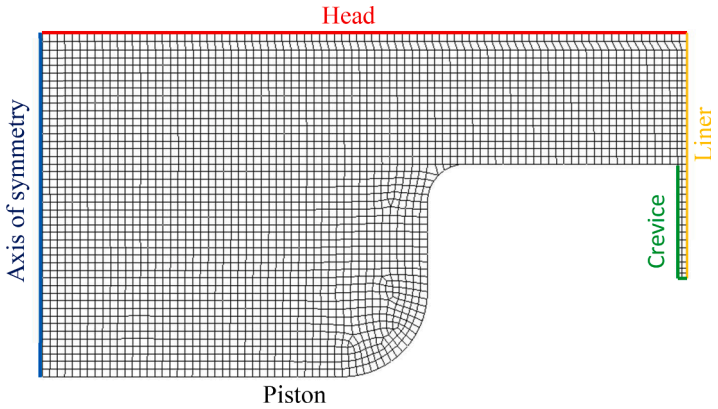

Fig. 1. Computational grid at 30 CAD BTDC.

modified as given in Ref. [58,59]. In this work, the constants are set to

$$C_\xi = 2.5652,\ C_\tau = 0.4368\ . \tag{9}$$

and have been slightly adjusted with respect to [56], to accurately simulate combustion in an HCCI engine. As regards the chemical kinetics, a skeletal kinetic mechanism for iso-octane [60], coupled with two sub-mechanisms for ozone [27] and nitrogen oxides [61], has been considered. Such a mechanism includes 187 chemical species in 931 reactions and it has already been successfully employed in a previous work of the authors [35].

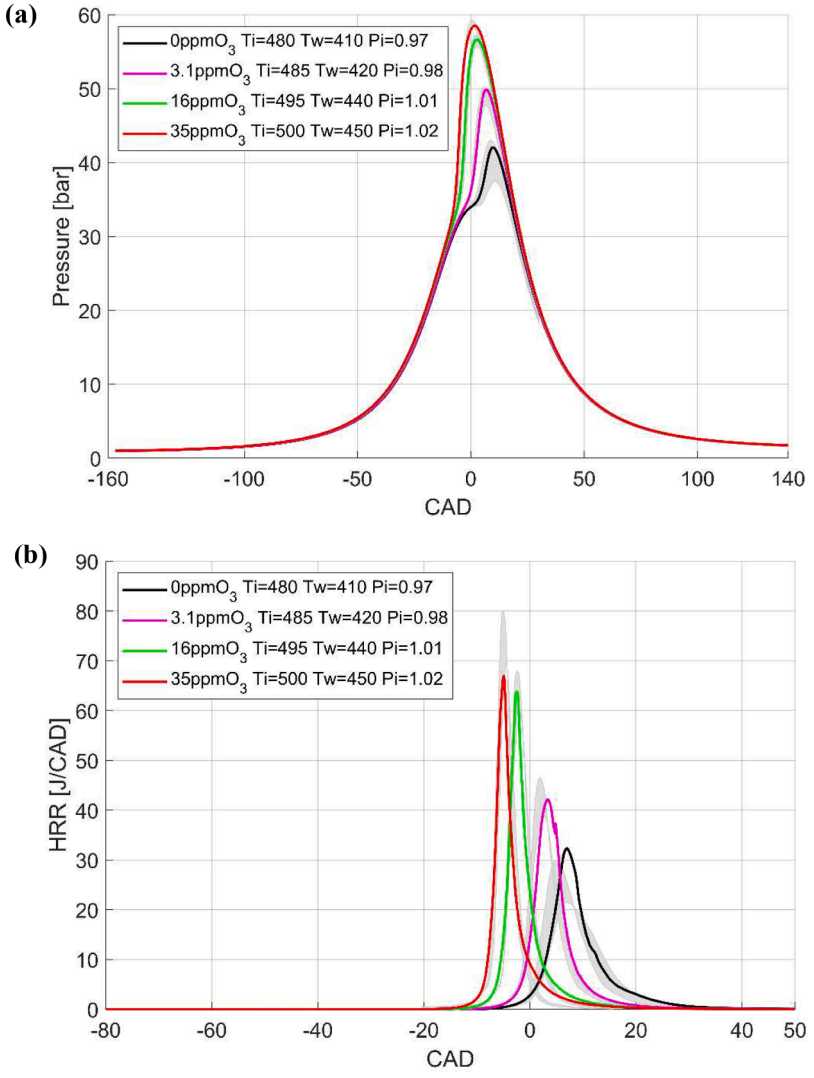

Fig. 2. Experimental (grey areas) and numerical results in terms of: (a) in-cylinder pressure; (b) heat release rate. In the legend, temperatures are in Kelvin and pressure in bar.

2.2. The test case and the numerical method

In order to validate the numerical model, an engine operating under HCCI conditions has been considered. This engine has already been experimentally investigated in Ref. [21]. The main characteristics of the engine are summarized in Table 1.

The vaporized iso-octane, air and ozone are mixed in a plenum located upstream of the intake manifold. The plenum is kept at a constant temperature of 473 K. The intake pressure is set to 1 bar. Ozone concentration is measured downstream of the plenum by using an ozone analyzer and is a function of the capacity of the ozone generator. The experimental data have been collected in terms of in-cylinder pressure, from 30 CAD BTDC to 30 CAD ATDC every 0.1 CAD, during 100 working cycles. Ozone concentration is equal to 0, 3.1, 16 and 35 ppm, corresponding to ozone generator capacity of 0, 5, 30 and 100 %, respectively. The heat release rate has been obtained from in-cylinder pressure profiles by means of thermodynamic considerations.

Numerical simulations are carried out with closed-valves, starting from intake valve closing (IVC = 157 CAD BTDC) to exhaust valve opening (EVO = 140 CAD ATDC). For instance, Fig. 1 shows the computational domain at 30 CAD BTDC.

As shown in Fig. 1, an axisymmetric 2-D computational domain has been considered. This geometrical simplification is needed to drastically reduce the computational time due to the detailed chemical kinetics, which is solved for each numerical time-step and each numerical cell. The combustion chamber consists of a flat head and a cup in the piston. Crevices are also simulated, whose thickness is equal to 0.6 mm and whose volume is equal to 3.46 % of the volume at TDC. The mesh is composed of quadrilateral elements, except for the region near the piston cup profile. The grid at IVC consists of 16,346 numerical cells and has been generated by setting an average cell size equal to 0.5 mm. The mesh motion has been obtained by using a well-proven layering technique described in both the theory and user's guide of the software [62, 63].

The simulations have been carried out by considering, at IVC, a homogeneous mixture of iso-octane, air, ozone and residual gases, that are a result of the previous working cycle with different mass percentages, i.e. 0, 5 and 10 %. As regards the residual gas compositions, they have been computed by using two procedures. The first approach concerns with the evaluation of the mass fractions of residuals given the equivalence ratio (ϕ) and the following global reaction:

$$C_8H_{18} + \frac{25}{2\phi}O_2 + 3.76*\frac{25}{2\phi}N_2 \rightarrow 8CO_2 + 9H_2O + \frac{25}{2\phi}(1-\phi)O_2 + 3.76*\frac{25}{2\phi}N_2, \tag{10}$$

In this case, the residual gas consists of CO_2, H_2O, O_2 and N_2, and hereafter this composition will be referred to as Simplified Mixture (SM). The second procedure takes into account a more accurate residual gas composition: a working cycle with SM composition at IVC has been initially simulated, and the gas composition obtained at Exhaust Valve Opening (EVO) has been used for the new working cycle. Only the chemical species whose amount is greater than 1 ppm are considered. The following system of equations is solved to compute the residual mass fractions at IVC with different amounts of residual gases, preserving the species mass ratio obtained at EVO of the previous working cycle:

$$\begin{cases} \sum_i Y_i^{'} = RG, \ i = 1, \ldots, N_s^{EVO} \\ \dfrac{Y_i^{'}}{Y_{i^*}^{'}} = a_i^{EVO}, \ i = 1, \ldots, N_s^{EVO} \ \wedge \ i \neq i^* \end{cases}, \tag{11}$$

where the unknowns $Y_i^{'}$ are the mass fractions of the i-th chemical species at IVC, N_s^{EVO} is the number of chemical species in the residual gases, RG is the ratio between the residual gases mass and the total mass in the chamber at IVC, $Y_{i^*}^{'}$ is the mass fraction of a specific chemical species in the mixture (N_2 is chosen in this work), and a_i^{EVO} is the ratio between the mass fraction of the i-th chemical species and the mass fraction of species i^* at EVO of the previous working cycle obtained with SM. In what follows, such composition of residual gases will be referred to as Extended Mixture (EM).

The ozone concentration in the iso-octane/air/ozone mixture has been set based on experimental measurements. The swirl ratio is equal to 1 with a rigid body profile. The initial conditions in terms of turbulent kinetic energy (k) and dissipation rate (ε) have been evaluated according to Ref. [64].

A numerical time-step equal to 0.1 CAD has been used except for the range from 80 CAD BTDC to 40 CAD ATDC, where the time-step has been reduced by a factor of 10 to improve the numerical accuracy at the end of the compression stroke and during combustion.

The initial gas temperature and pressure, and the wall boundary conditions are discussed in detail in the following section.

3. Results and discussion

3.1. Model validation

The validation of the model has been carried out by comparing the computed in-cylinder pressure profiles, the corresponding heat release rate profiles and the polluting emissions with measured data available in Ref. [21].

Fig. 2 shows the numerical pressure and heat release rate profiles. The grey colored region represents the uncertainties of the experimental measurements during 100 working cycles. In the figure, the legend

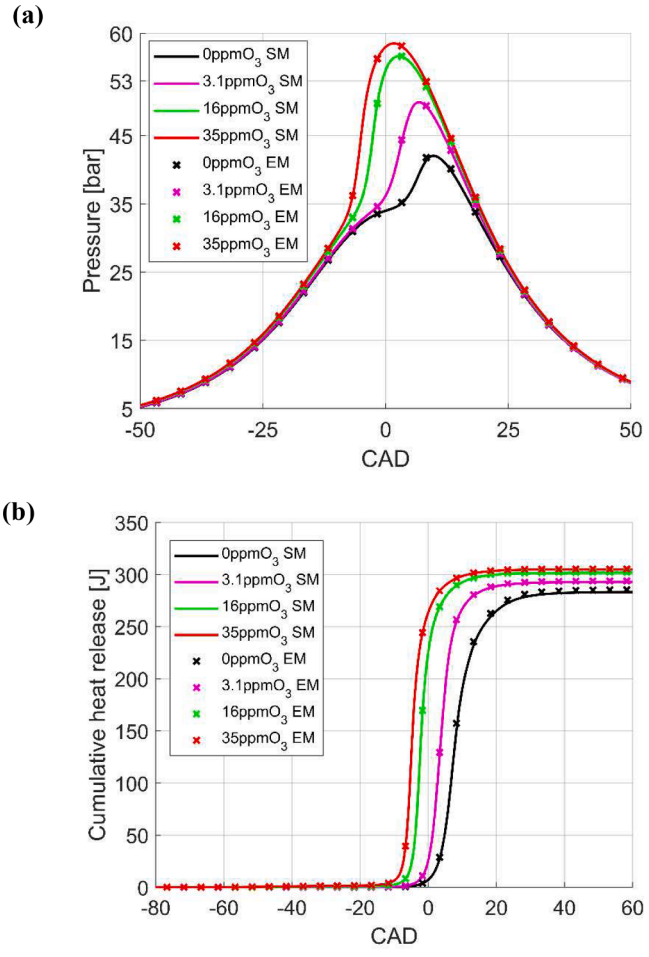

Fig. 3. Results with the simplified mixture (SM) and the extended mixture (EM): (a) in-cylinder pressure; (b) cumulative heat release.

shows the temperature (T_i) and pressure (P_i) at IVC and the wall temperature (T_w) for all the cases under investigation. Five percent by mass of residual gases have been considered with the simplified composition (SM).

As shown in Fig. 2, initial and boundary conditions have been adjusted for different ozone concentrations at IVC, since ozone influences the combustion process and, therefore, pressure and heat release rate profiles. Without ozone, large cycle-to-cycle variations occur and combustion efficiency is low: the heat released is, on average, more than 16 % lower than that of the case when 35 ppm of ozone are added to the mixture. Therefore, initial and boundary conditions need to be adjusted depending on the case. Specifically, T_i and T_w have been increased with ozone concentration and initial pressure has been adjusted to get nearly the same mass at IVC for all cases.

Fig. 2 shows a very good agreement between experimental data and numerical pressure profiles. As regards HRR profiles, a good agreement with experimental data is obtained, especially in the cases with low cycle-to-cycle variations, i.e. with 35 and 16 ppm of ozone. However, it should be considered that the experimental data in terms of HRR have been derived from pressure values using specific thermodynamic assumptions.

The computed pressure peak occurs, without ozone, at about 9.8 CAD ATDC, whereas, for the case with 35 ppm ozone, the pressure peak is advanced at 1.5 CAD ATDC. The peak values are 42 and 58.5 bar, respectively. As regards HRR profiles, without ozone, the HRR peak occurs at about 7 CAD ATDC and is equal to 32.3 J/CAD, and CA50 (crank angle position at which 50 % of the total heat is released) is 7.8 CAD ATDC. For the case with 35 ppm of ozone, the HRR peak occurs at 5 CAD BTDC and is equal to 67.2 J/CAD, and CA50 is 4.7 CAD BTDC. Following the experiments, the computed combustion efficiency varies with ozone concentrations. Specifically, the total heat released is 283 J, 293.5 J, 302.2 J and 305.4 J in the cases with 0, 3.1, 16 and 35 ppm of ozone, respectively.

Another set of simulations has been carried out under the same initial and boundary conditions, with the species composition at IVC obtained by considering the EM composition for the residual gases. Specifically, all species with a concentration above 1 ppm at EVO have been considered for each case. The results are very similar to those obtained with the SM composition, as shown in Fig. 3. Indeed, the pressure profiles differ by a maximum of 0.46 bar for the case without ozone at 7

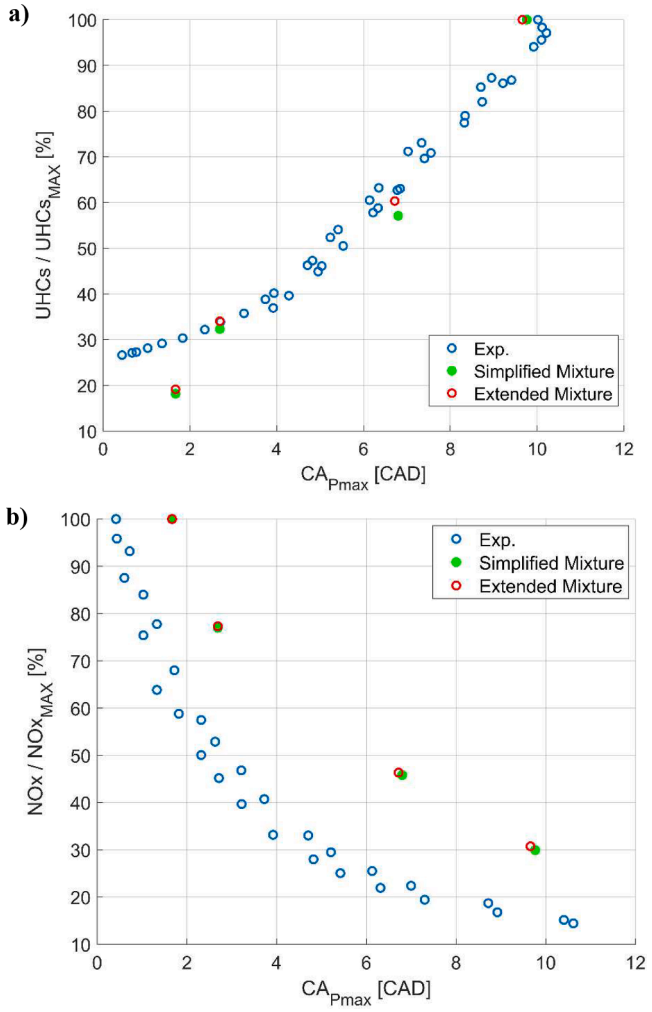

Fig. 4. Experimental and numerical normalized exhaust pollutants vs CA_{Pmax} with the SM and the EM approaches: (a) unburned hydrocarbons (UHCs); (b) nitrogen oxides (NO_x).

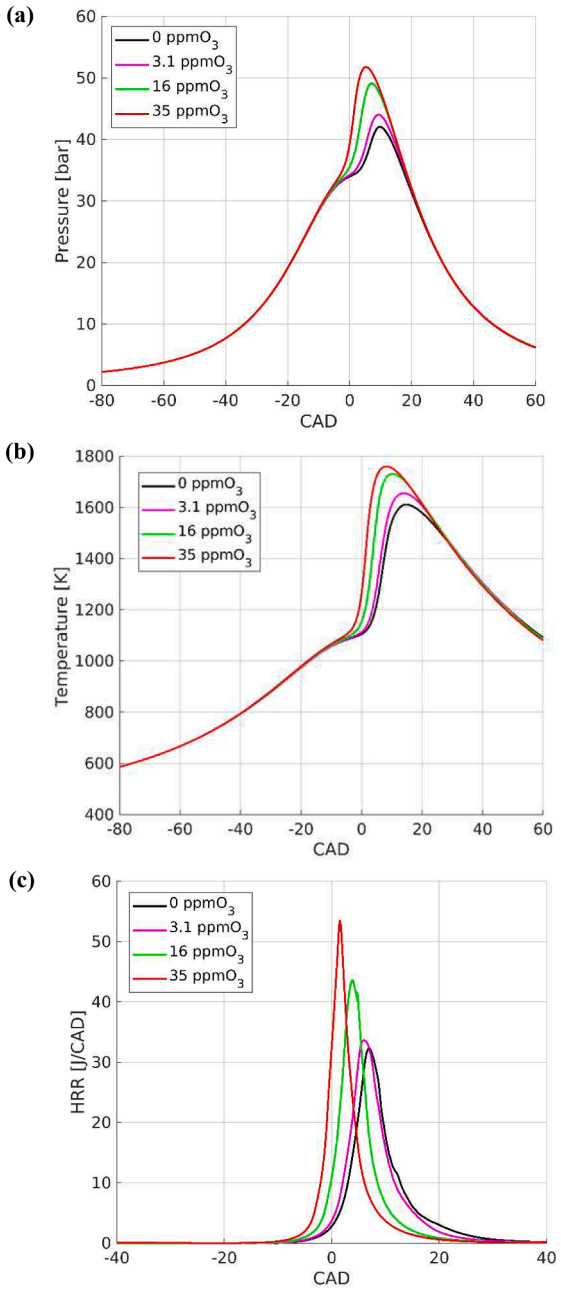

Fig. 5. Numerical results with $T_i = 480\ K$, $T_w = 410\ K$, $P_i = 0.97\ bar$ for different ozone concentrations: (a) in-cylinder pressure; (b) in cylinder-temperature; (c) heat release rate.

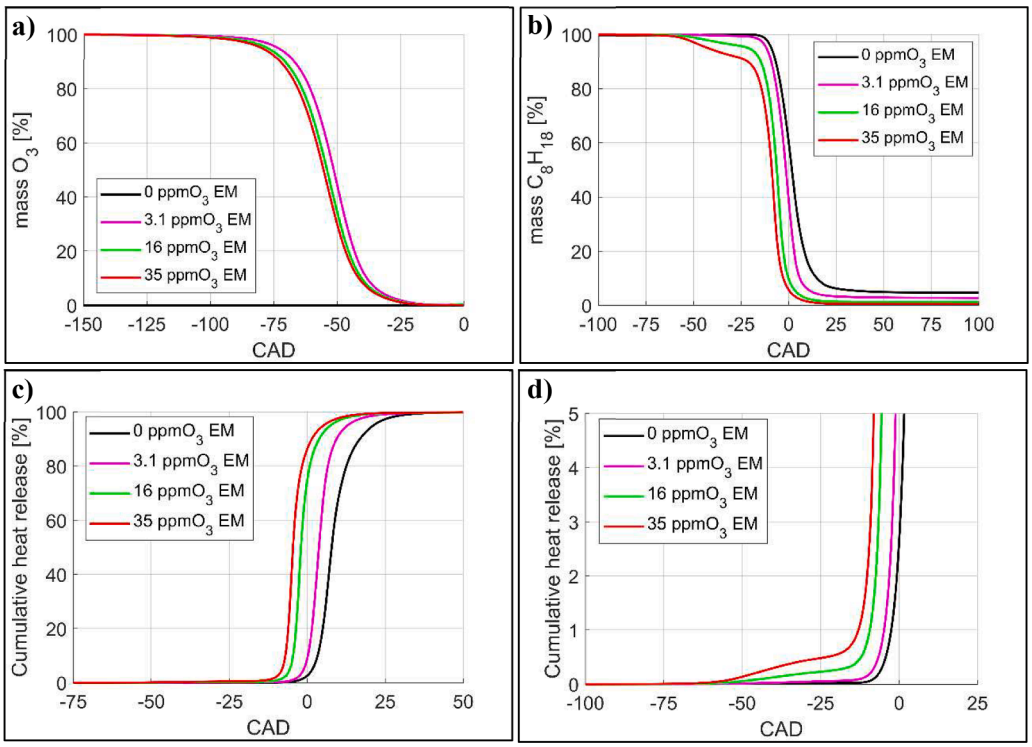

Fig. 6. Profiles of a) ozone; b) isooctane; c) cumulative heat release; d) blow-up of cumulative heat release as a function of CAD with 5 % by mass of residual gases and different ozone concentrations.

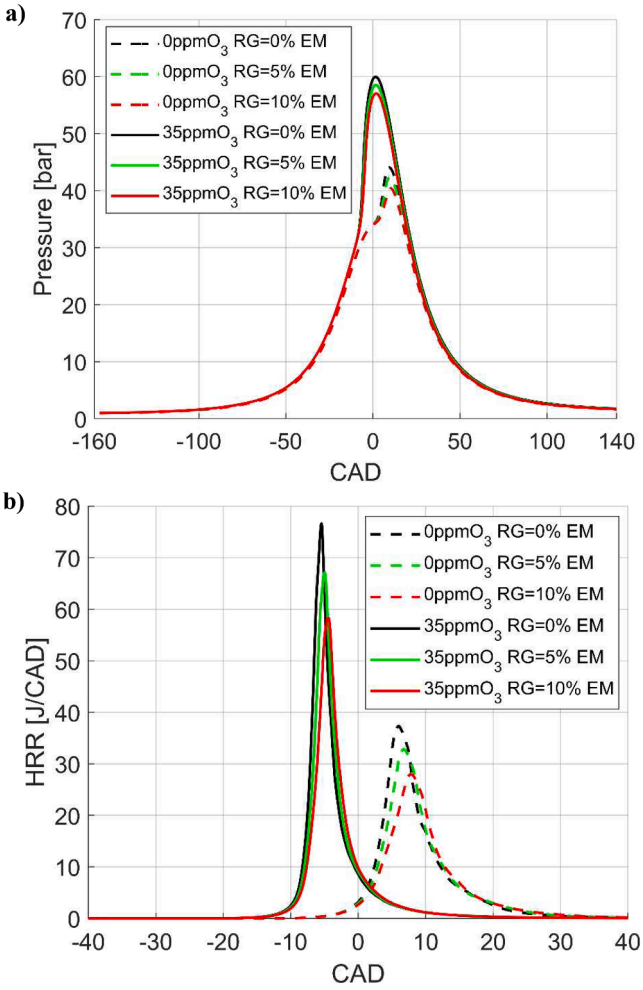

Fig. 7. Numerical results with different ozone concentrations and residual gases mass fractions (RG): (a) in-cylinder pressure; (b) heat release rate.

CAD ATDC, the HRR profiles differ by a maximum of 1.89 J for the case without ozone at 5.9 CAD ATDC and the largest difference in terms of the total heat released is 2 J and occurs in the absence of ozone.

Fig. 4 shows the normalized values of exhaust pollutants, in terms of both unburned hydrocarbons (UHCs) and nitrogen oxides (NO_x), as a function of the crank angle at which the pressure peaks occur (CA_{Pmax}), with both SM and EM approaches. The value of CA_{Pmax} is related to the capacity of the ozone generator. Specifically, as the ozone concentration increases, the pressure peak advances, as shown in Fig. 2(a).

The numerical results show an overall good agreement with experiments in terms of UHCs, with small differences between the simplified and extended approaches. As the ozone concentration increases (i.e. CA_{Pmax} decreases), unburned hydrocarbons concentration decreases up to about 26 % and 19 % with respect to the measured and computed concentrations, respectively, without ozone. For instance, for the case without ozone, a percentage of about 4.66 % and 5 % of the initial hydrocarbons mass remains unburned by employing the extended and simplified procedures, respectively. On the other hand, for the case with 35 ppm of ozone, these percentages drop to 0.47 % and 0.46 %, respectively. This unburned mass is mainly the fuel trapped in the crevices, where no combustion occurs.

Furthermore, nitrogen oxides decrease as the ozone concentration decreases, i.e. CA_{Pmax} increases. As NO_x are produced by the high local temperatures reached in the chamber, a larger amount of nitrogen oxides is found where combustion is faster and more complete. The SM and EM procedures give similar results. Some discrepancies between numerical and experimental results in terms of the amount of nitrogen oxides are observed, mainly as ozone concentration decreases. These differences may be related to the measured cycle-to-cycle variability. Indeed, as shown in Fig. 2(a), for the cases without and with 3.1 ppm ozone, the computed pressure traces are located in the upper part of the respective experimental shadow regions, and this leads to a more efficient combustion and, consequently, to a higher NO_x production.

To ensure that the model is able to assess the influence of ozone on combustion, and that the above results are not merely the outcome of *ad-hoc* initial and boundary conditions, a set of simulations have also been carried out for different initial ozone concentrations, by keeping the same initial and boundary conditions in terms of gas pressure and temperature, i.e. $T_i = 480\ K$, $T_w = 410\ K$, $P_i = 0.97\ bar$. Fig. 5 shows the results in terms of pressure, mass-averaged in-cylinder temperature and heat release rate. The results show trends similar to those of Fig. 2, but less pronounced. Specifically, with 35 ppm ozone, the pressure peak increases by 10 bar and occurs 4.7 CAD earlier than the case without ozone. In addition, the auto-ignition timing is advanced by about 5 CAD and the HRR peak is advanced by about 5.5 CAD and increases by 22 J/CAD. The average in-cylinder temperature reaches a maximum value of 1760 K with 35 ppm ozone, that is 150 K greater than that of the case without ozone.

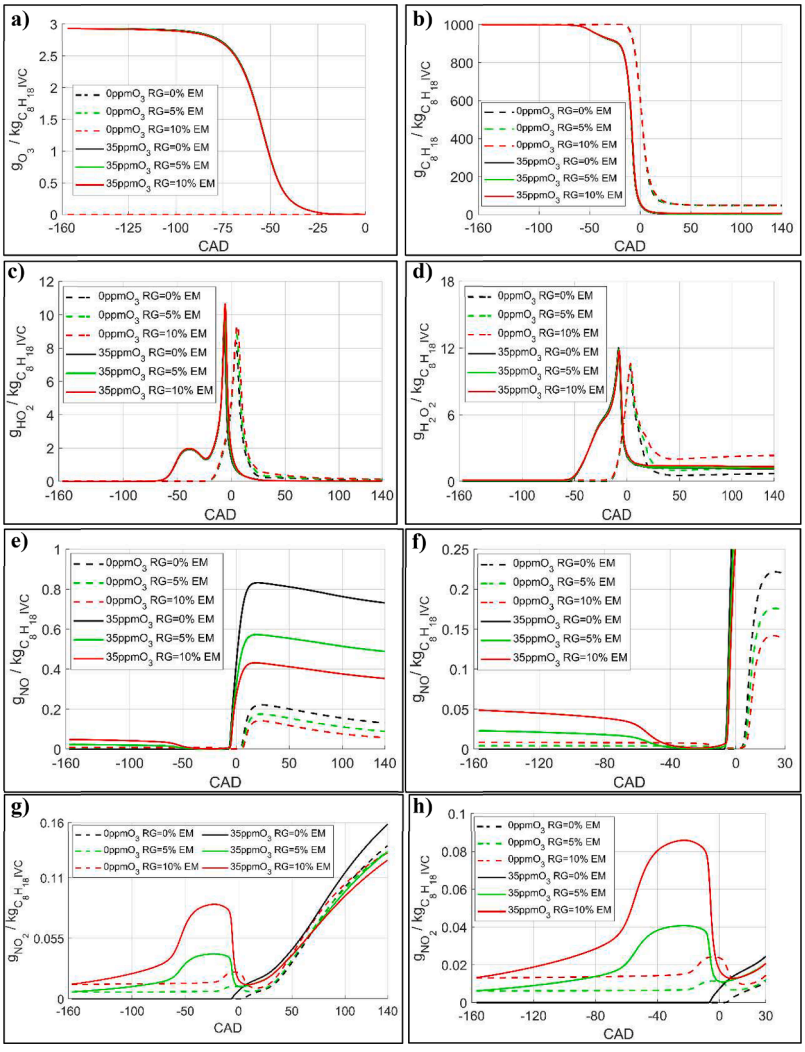

Fig. 8. Numerical results with different ozone concentrations and residual gases mass fractions (RG) in terms of species mass divided by the initial fuel mass (C_8H_{18} at IVC) vs CAD: a) O_3; b) C_8H_{18}; c) HO_2; d) H_2O_2; e) NO; f) NO, blow-up; g) NO_2; h) NO_2, blow-up.

3.2. Influence of ozone and residual gas

The combined influence of ozone and residual gas on the combustion in the HCCI engine has been analyzed by varying the ozone concentration in the range 0–35 ppm and the residual gases mass fraction in the range 0–10 %. For such a study, the EM approach is used, since it includes combustion intermediates and partially oxidized and/or reactive species that could potentially interact with ozone during compression.

Fig. 6 shows ozone, fuel and heat release profiles as a function of CAD with different ozone concentrations and with the same amount of residual gases (5 % by mass).

Fig. 6(a) and (b) show that both ozone and fuel are depleted during the compression stroke. Specifically, ozone depletion is mainly due to the reaction $O_3 + N_2 \rightleftarrows O_2 + O + N_2$, as discussed in Ref. [24,31,35,65,66]. Such a reaction is favored by the higher temperature reached by increasing the ozone concentration. Specifically, up to 100 CAD BTDC for all cases, the ozone concentration is almost the same as that at IVC. At 60 CAD BTDC the mass of ozone reduces to 79 %, 70.7 % and 66.2 % with initial ozone concentrations equal to 3.1 ppm, 16 ppm and 35 ppm, respectively. Finally, at 20 CAD BTDC, the mass of ozone is less than 1 % for all cases.

The availability of oxygen atoms, produced by the ozone depletion process, enables the reaction $C_8H_{18} + O \rightarrow C_8H_{17} + OH$ and, subsequently, the reaction $C_8H_{18} + OH \rightarrow C_8H_{17} + H_2O$, that both convert the fuel to C_8H_{17} before auto-ignition. As shown in Fig. 6(b), iso-octane starts to be depleted earlier and to a greater extent for the cases with higher ozone concentrations. Specifically, at 20 CAD BTDC the mass percentage of isooctane is 89.2 %, 94.7 %, 99.2 % and 100 % of the amount available at IVC for the cases with 35 ppm, 16 ppm, 3.1 ppm and 0 ppm of ozone, respectively. The above chemical reactions, in addition to leading to the production of radicals and intermediate chemical species, cause an acceleration of the chemical kinetics and a release of a certain amount of heat along the initial stage of combustion. Indeed, as shown in Fig. 6(d), for all cases with ozone, a small amount of heat is released before main combustion takes place.

In order to analyse how ozone reacts with residual gases, computations have also been carried out by varying the amount of residual gas, i.e. 0 %, 5 % and 10 % by mass, for cases with 0 ppm and 35 ppm of ozone. The initial and boundary conditions are those described in Section 3.1. Fig. 7 shows the results of the simulations in terms of pressure and heat release rate profiles as a function of CAD. Figs. 8 and 9 show the mass profiles of some relevant chemical species, divided by the initial fuel mass, as a function of CAD. Finally, the combustion parameters CA10, CA50, CA90, the combustion duration and the total heat released are summarized in Table 2, by computing the combustion duration as the difference between CA90 and CA10 (i.e. the crank angles when 10 % and 90 % of the total heat has been released, respectively).

Fig. 7(a) shows that, for a given ozone concentration, an increase of the mass percentage of residual gases at IVC reduces the pressure peak in the chamber due to the less amount of fuel available at IVC. As a consequence, less heat is released, as shown in Table 2. As regards the combustion process, both Fig. 7(b) and Table 2 show that combustion duration is shorter as the percentage of residual gases decreases, both without ozone and with the addition of 35 ppm of O_3. Specifically, the lower amount of residual gases also leads to an advance of the overall combustion process, as it can be seen by considering CA10, CA50 and CA90 of Table 2.

Fig. 8(a) and (b) show that the depletion of both ozone and fuel is comparable for the same ozone concentration and different residual gases mass percentages. However, ozone depletion is slightly faster for cases with a higher amount of residual gases, whereas the opposite occurs for fuel. Indeed, for the cases with 35 ppm of ozone, at 90 CAD BTDC, 2.88 and 2.86 g_{O_3}/kg_{fuel} are found in the chamber with 0 % and 10 % of residual gases, respectively. Conversely, at 30 CAD BTDC, 92 % and 94 % of the initial fuel is still in the chamber with 0 % and 10 % of

Table 2
Combustion parameters for the cases with 0 and 35 ppm of ozone and 0 %, 5 % and 10 % by mass of residual gases (RG) at IVC.

	$Value_{0ppmo_3}$ / $Value_{35ppmo_3}$		
	RG = 0 %	**RG = 5 %**	**RG = 10 %**
CA10 [CAD]	+3.09 / −7.29	+3.30 / −7.05	+3.49 / −6.81
CA50 [CAD]	+7.16 / −5.04	+7.82 / −4.59	+8.62 / −4.09
CA90 [CAD]	+15.69 / +1.02	+16.83 / +1.44	+17.69 / +1.94
CA90-CA10 [CAD]	12.6 / 8.31	13.53 / 8.49	14.2 / 8.75
Total heat release [J]	302 / 323	286 / 306	266 / 289

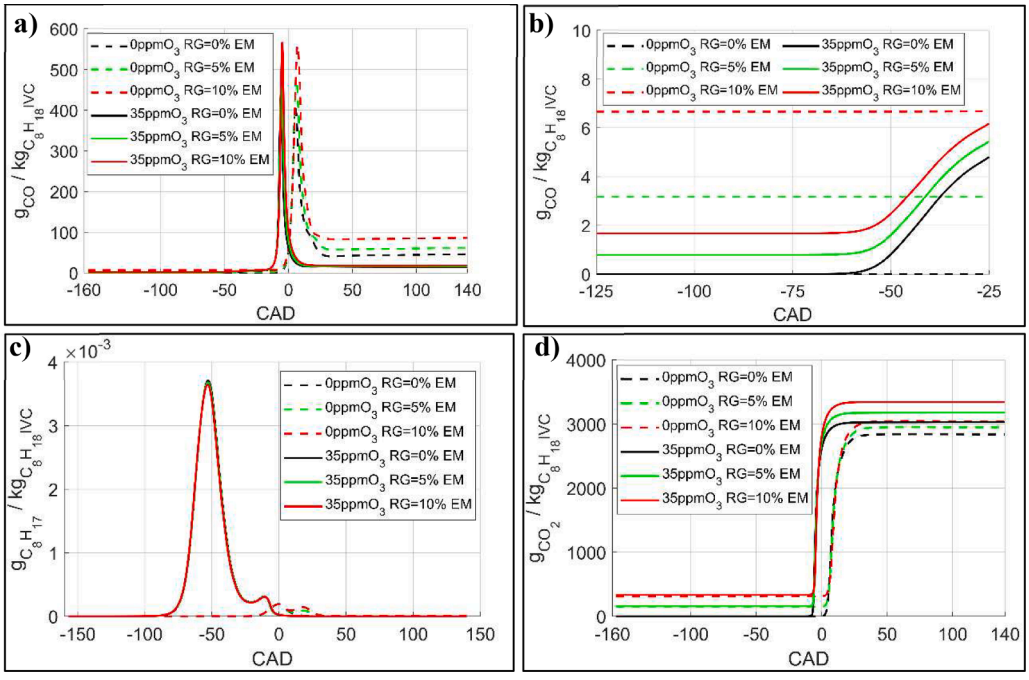

Fig. 9. Numerical results with different ozone concentrations and residual gases mass fractions (RG) in terms of species mass divided by the initial fuel mass (C_8H_{18} at IVC) vs CAD: a) *CO*; b) *CO*, blow-up; c) C_8H_{17}; d) CO_2.

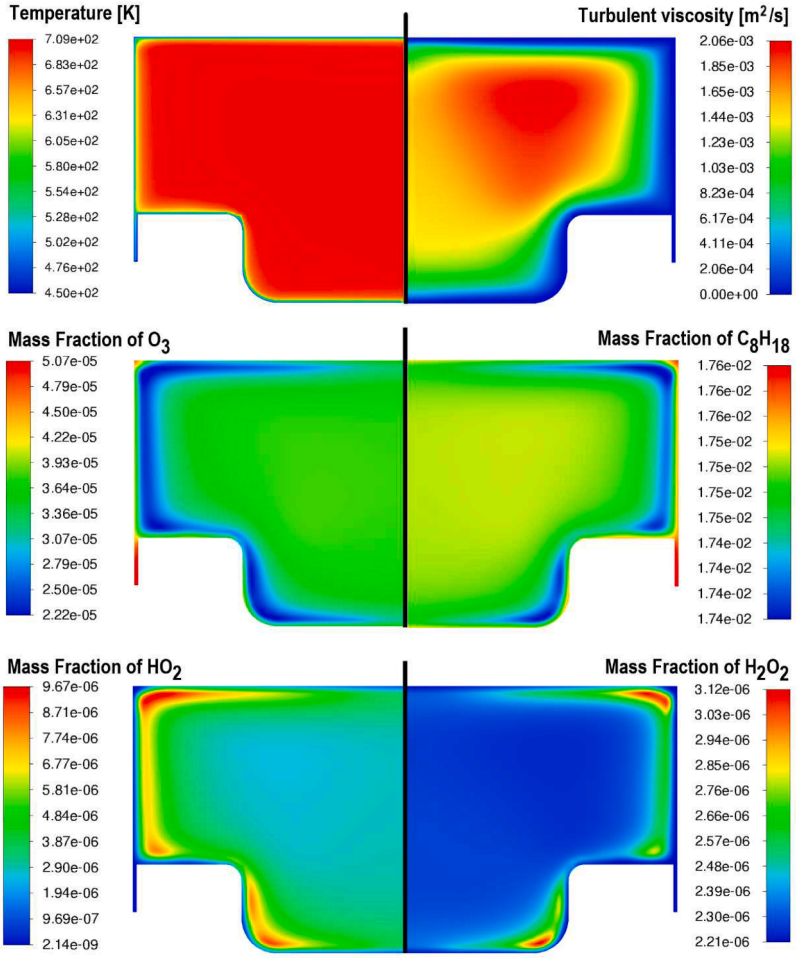

Fig. 10. In-cylinder contour plots at 60 CAD BTDC for the case with 35 ppm of ozone and 10 % by mass of residual gases at IVC.

residual gases, respectively.

Moreover, Fig. 8(c) and (d) show that, for the cases with 35 ppm of O_3, as ozone starts to deplete, HO_2 and H_2O_2 are produced. This is typically associated with the LTC regime, which leads to an early mixture auto-ignition. Fig. 10 shows the contour plots of temperature, turbulent viscosity, and mass fractions of O_3, C_8H_{18}, HO_2 and H_2O_2 at 60 CAD BTDC for the case with 35 ppm of ozone and 10 % by mass of residual gases at IVC. The in-cylinder temperature is fairly uniform, except for regions near walls and crevices, and the maximum value ($\approx$ 709 K) occurs in the center of the chamber. However, ozone depletion, and consequently fuel oxidation and the production of HO_2 and H_2O_2 radicals, start in the regions of the chamber with high thermal gradients, but reasonably far from the walls (temperature is still above 675 K). This result is in agreement with those obtained in both numerical and experimental findings in the literature concerning HCCI engines combustion [15,16,66,67].

In the presence of residual gases, ozone reacts not only through the reaction $O_3 + N_2 \rightleftarrows O_2 + O + N_2$, but also with other species, such as nitrogen monoxide, through the reaction $NO + O_3 \rightarrow NO_2 + O_2$ with reactants molar ratio equal to 1:1. In Fig. 8(e)–(h), it can be observed that, without ozone, the mass of both nitrogen monoxide and nitrogen dioxide remains the same up to about 20 CAD BTDC. Then, in the LTC regime, as shown in Fig. 8(f) and (h), nitrogen monoxide is oxidized to NO_2 and, as temperature starts to rise very fast due to the increase of HRR, more nitrogen monoxide is produced and NO_2 partially dissociates (from 20 CAD BTDC to 10 CAD ATDC). Finally, NO_2 is produced again by NO oxidation. On the other hand, in the presence of ozone, at IVC NO is immediately converted into NO_2, with a higher rate at 70 CAD BTDC, i.e. as a faster depletion of ozone occurs. This process is also shown in Fig. 11, where the in-cylinder distribution of NO and NO_2 at 30 CAD BTDC are given for the cases with and without ozone addition and with 10 % by mass of residual gases. Specifically, the highest concentration of NO is observed in the center of the chamber for both cases, i.e. without ozone and with 35 ppm ozone at IVC, whereas the opposite occurs for NO_2. This is because NO production and NO_2 dissociation are promoted by high temperature values, which occur in the center of the chamber. However, for the case without ozone, these two species are distributed quite uniformly in the chamber, except for the near-wall regions. On the other hand, for the case with ozone addition, the stratification is more pronounced and, except for the crevices, NO concentration is lower than the case without ozone. This is because NO reacts with O_3 to produce NO_2, but the reaction between O_3 and NO occurs much more slowly in the crevices, due to the lower temperature than that of other regions. The reaction $NO + O_3 \rightarrow NO_2 + O_2$ reduces the amount of ozone for the production of oxygen atoms in the pre-heating zone, even if this reaction is not the only responsible for such a depletion. Indeed, for the case with 35 ppm of ozone and 10 % of residual gases, at IVC the mass of NO and ozone are 0.32 μg and 19.25 μg, respectively. Thus, the reaction $NO + O_3 \rightarrow NO_2 + O_2$ depletes less than 3 % by mass of the initial amount of O_3.

The oxygen atoms produced by the reaction $O_3 + N_2 \rightleftarrows O_2 + O + N_2$, being highly reactive, oxidise not only the fuel but many of the intermediate species of the residual gas. As shown in Fig. 9(a)–(c), there is a production of both C_8H_{17} (i.e. $C_8H_{18} + O \rightleftarrows C_8H_{17} + OH$) and CO, which corresponds to a faster ozone depletion. Specifically, for the cases with ozone and with 10 % of residual gases, the peak of C_8H_{17} is 1.73 % lower

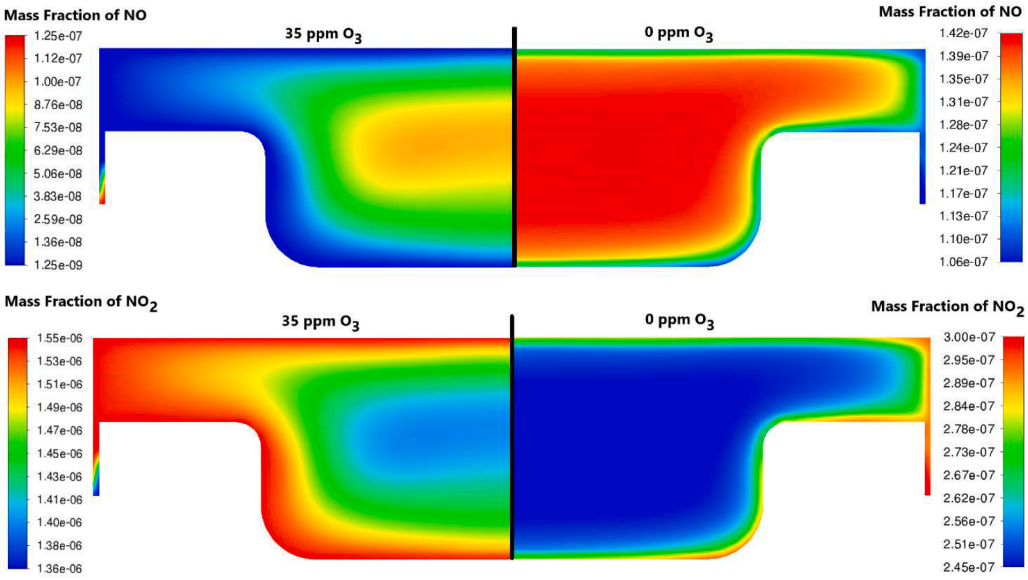

Fig. 11. In-cylinder contour plots of *NO* and NO_2mass fraction at 30 CAD BTDC for the cases with 10 % by mass of residual gases at IVC, with 35 ppm ozone at IVC (left) and without ozone addition (right).

Table 3
Engine performance parameters with different ozone concentrations and residual gases mass fractions (RG) at IVC.

	$\text{Value}_{0ppm_{O_3}} / \frac{\text{Value}_{35ppm_{O_3}} - \text{Value}_{0ppm_{O_3}}}{\text{Value}_{0ppm_{O_3}}} * 100$		
	RG = 0 %	RG = 5 %	RG = 10 %
$W^g_{c,I}$ [J]	141.5 / +2.52 %	132.4 / +3.58 %	122.2 / +5.7 %
$IMEP^g$ [bar]	2.83 / +2.52 %	2.65 / +3.58 %	2.45 / +5.7 %
$\dot{P}^g_I$ [kW]	1.77 / +2.52 %	1.66 / +3.58 %	1.53 / +5.7 %
SFC^g [g/kWh]	184.26 / −1.54 %	187.35 / −2.77 %	192.65 / −4.96 %

than for the case without residual gases, due to a lower amount of oxygen atoms that react with iso-octane.

Finally, the engine performance parameters have been computed for the cases with different ozone concentrations and residual gases at IVC. The results are given in Table 3 in terms of i) the gross indicated work per cycle, $W^g_{c,I}$, defined as the work delivered to the piston along the compression and expansion strokes, computed as: $W^g_{c,I} = \int_{IVC}^{EVO} PdV$; ii) the gross Indicated Mean Effective Pressure, $IMEP^g$, computed as: $IMEP^g = \frac{W^g_{c,I}}{V_c}$; iii) the gross indicated power output, $\dot{P}^g_I$, computed as: $\dot{P}^g_I = W^g_{c,I} * \frac{RPM}{60 n_{rc}}$ where n_{rc} is the number of revolutions per working cycle; and iv) the gross Specific Fuel Consumption, SFC^g, computed as: $SFC^g = \frac{M_{fuel_{IVC}}}{W^g_{c,I}}$, where $M_{fuel_{IVC}}$ is the fuel mass at IVC, which is related to the gross thermodynamic efficiency of the cycle, η^g_{th}, by: $\eta^g_{th} = \frac{1}{H_{i,fuel} SFC^g}$ where $H_{i,fuel}$ is the lower calorific value of the fuel.

The results show that ozone increases the engine performances and reduces the specific fuel consumption. The influence of ozone is more evident for cases with a higher percentage of residual gases. Furthermore, with the addition of 35 ppm ozone, combustion duration is reduced by 34.05 %, 37.25 % and 38.38 % for the cases with 0 %, 5 % and 10 % in mass of residual gases, respectively. Despite the presence of chemical species (e.g. nitrogen monoxide) that could limit the effectiveness of ozone, their influence is negligible due to their small concentration. On the other hand, the benefit of ozone is greater for cases with a higher percentage of residual gases, since the amount of fuel decreases by increasing the residual gases mass fraction, which slows down the combustion process.

4. Conclusions

In this work, the influence of ozone addition in an HCCI engine fuelled with iso-octane has been investigated. Specifically, a parametric analysis has been carried out by varying the mass of residual gases in the chamber, with the aim of understanding the combined effect of ozone and residual gases. For this purpose, CFD simulations of a closed-valve engine cycle have been carried out, by solving the chemistry with a kinetic mechanism with 187 chemical species and 931 reactions. The model has been validated against experimental data available in the literature in terms of in-cylinder pressure profiles, heat release rate profiles and pollutants. The final considerations are:

- Ozone addition (from 3 to 30 ppm) advances mixture auto-ignition and reduces combustion duration. Combustion is also more complete, leading to a reduction in UHCs but to an increase of NO_x, due to the higher temperatures reached in the chamber.
- Ozone decomposes during the engine compression stroke, releasing oxygen atoms, which oxidize fuel and other intermediate species. This enables Low-Temperature Combustion with the release of species such as *OH*, HO_2 and H_2O_2. Reactions in the LTC regime also result in a small amount of heat being released before the occurrence of auto-ignition.
- As the percentage of residual gas increases, more ozone is depleted by reacting with nitrogen oxide in the chamber through the reaction $NO + O_3 \rightarrow NO_2 + O_2$. In addition, some of the oxygen atoms produced by the reaction $O_3 + N_2 \rightleftarrows O_2 + O + N_2$ react with other intermediate species instead of fuel. However, the amount of the chemical species that could limit the effectiveness of ozone is not enough to alter the benefits of using ozone.
- As expected, without ozone, engine performance is reduced by increasing the amount of residual gas. However, ozone effect is larger by increasing the percentage of residual gas. Specifically, with an ozone concentration of 35 ppm at IVC, the gross work per cycle increases by 2.52 %, 3.58 % and 5.7 %, compared to the case without ozone, by using 0 %, 5 % and 10 % by mass of residual gases; on the other hand, the specific fuel consumption is reduced by 1.54 %, 2.77 % and 4.96 % for the same cases.

CRediT authorship contribution statement

Marco D'Amato: Investigation, Methodology, Software, Validation, Visualization, Writing – original draft, Conceptualization, Data curation, Formal analysis. **Vinicio Magi:** Funding acquisition, Investigation, Methodology, Resources, Software, Supervision, Writing – review & editing. **Annarita Viggiano:** Funding acquisition, Investigation, Validation, Writing – review & editing, Methodology, Project administration, Resources, Software, Supervision, Conceptualization.

Declaration of competing interest

The authors declare that they have no known competing financial interests or personal relationships that could have appeared to influence the work reported in this paper.

Data availability

Data will be made available on request.

References

[1] H. Ritchie, M. Roser, P. Rosado, Energy, Published online at OurWorldInData.org. (2022), https://ourworldindata.org/energy. Accessed June 2023.
[2] International Energy Outlook (IEO) (2021), [Online Resource] https://www.eia.gov/outlooks/ieo/. Accessed June 2023.
[3] H. Ritchie, M. Roser, P. Rosado, CO2 and greenhouse gas emissions, Published online at OurWorldInData.org. (2020), https://ourworldindata.org/co2-and-other-greenhouse-gas-emissions. Accessed June 2023.
[4] IEA, Transport sector CO2 emissions by mode in the sustainable development scenario, 2000-2030, IEA, Paris https://www.iea.org/data-and-statistics/charts/transport-sector-co2-emissions-by-mode-in-the-sustainable-development-scenario-2000-2030 (2019), IEA. Licence: CC BY 4.0. Accessed June 2023.
[5] R.D. Reitz, Directions in internal combustion engine research, Combust. Flame 160 (2013) 1–8.
[6] S. Imtenan, M. Varman, H.H. Masjuki, M.A. Kalam, H. Sajjad, M.I. Arbab, I. M. Rizwanul Fattah, Impact of low temperature combustion attaining strategies on diesel engine emissions for diesel and biodiesels: a review, Energy Convers. Manag. 80 (2014) 329–356.
[7] H. Bendu, S. Murugan, Homogeneous charge compression ignition (HCCI) combustion: mixture preparation and control strategies in diesel engines, Renew. Sustain. Energy Rev. 38 (2014) 732–746.
[8] M.M. Hasan, M.M. Rahman, Homogeneous charge compression ignition combustion: advantages over compression ignition combustion, challenges and solutions, Renew. Sustain. Energy Rev. 57 (2016) 282–291.
[9] T.K. Sharma, G.A.P. Rao, K.M. Murthy, Homogeneous charge compression ignition (HCCI) engines: a review, Arch. Comput. Method. E 23 (2016) 623–657.
[10] J.E. Dec, M. Sjöberg, Isolating the effects of fuel chemistry on combustion phasing in an HCCI engine and the potential of fuel stratification for ignition control, SAE Tech. Paper (2004) 2004-01-0557.
[11] F. Maroteaux, E. Mancaruso, M. Vaglieco, Optical and numerical investigations on combustion and OH radical behavior inside an optical engine operating in LTC combustion mode, Energies 16 (2023) 3459.
[12] S. Saxena, I.D. Bedoya, Fundamental phenomena affecting low temperature combustion and HCCI engines, high load limits and strategies for extending these limits, Prog. Energy Combust. 39 (2013) 457–488.
[13] S. Gowthaman, A.P. Sathiyagnanam, Analysis the optimum inlet air temperature for controlling homogeneous charge compression ignition (HCCI) engine, Alex. Eng. J. 57 (2018) 2209–2214.
[14] B. Prasad, C. Sharma, T. Anand, R. Ravikrishna, High swirl-inducing piston bowls in small diesel engines for emission reduction, Appl. Energy 88 (2011) 2355–2367.
[15] M. D'Amato, A. Viggiano, V. Magi, On the turbulence-chemistry interaction of an HCCI combustion engine, Energies 13 (2020) 5876.
[16] M. Christensen, B. Johansson, A. Hultqvist, The effect of combustion chamber geometry on HCCI operation, SAE Tech. Paper (2002) 2002-01-0425.
[17] E. Distaso, R. Amirante, G. Calò, P. De Palma, P. Tamburrano, R.D. Reitz, Predicting lubricant oil induced pre-ignition phenomena in modern gasoline engines: the reduced GasLube reaction mechanism, Fuel 281 (2020) 118709.
[18] D. Jung, N. Iida, Closed-loop control of HCCI combustion for DME using external EGR and rebreathed EGR to reduce pressure-rise rate with combustion-phasing retard, Appl. Energy 138 (2015) 315–330.
[19] M. Sjoberg, J.E. Dec, W. Hwang, Thermodynamic and chemical effects of EGR and its constituents on HCCI autoignition, SAE Tech. Paper (2007) 2007-01- 0207.
[20] F. Foucher, P. Higelin, C. Mounaïm-Rousselle, P. Dagaut, Influence of ozone on the combustion of n-heptane in a HCCI engine, Proc. Combust. Inst. 34 (2013) 3005–3012.
[21] J.-B. Masurier, F. Foucher, G. Dayma, C. Rousselle, P. Dagaut, Application of an ozone generator to control the homogeneous charge compression ignition combustion process, SAE Tech. Paper (2015) 2015-24-2456.
[22] J.-B. Masurier, F. Foucher, G. Dayma, P. Dagaut, Homogeneous charge compression ignition combustion of primary reference fuels influenced by ozone addition, Energy Fuels 27 (2013) 5495–5505.
[23] J.-B. Masurier, F. Foucher, G. Dayma, P. Dagaut, Investigation of iso-octane combustion in a homogeneous charge compression ignition engine seeded by ozone, nitric oxide and nitrogen dioxide, Proc. Combust. Inst. 35 (2015) 3125–3132.
[24] W. Sun, X. Gao, B. Wu, T. Ombrello, The effect of ozone addition on combustion: kinetics and dynamics, Prog. Energy Combust. Sci. 73 (2019) 1–25.
[25] J. McClurkin, D. Maier, Half-life time of ozone as a function of air conditions and movement, Julius-Kühn-Archiv 25 (2010) 381.
[26] T. Nomaguchi, S. Koda, Spark ignition of methane and methanol in ozonized air, Symp. (Int.) Combust. 22 (1989) 1677–1682.
[27] F. Halter, P. Higelin, P. Dagaut, Experimental and detailed kinetic modeling study of the effect of ozone on the combustion of methane, Energy Fuels 25 (2011) 2909–2916.
[28] T. Ombrello, S.H. Won, Y. Ju, S. Williams, Flame propagation enhancement by plasma excitation of oxygen. Part I: effects of O3, Combust. Flame 157 (2010) 1906–1915.
[29] W. Xie, S. Drost, R. Schiebl, U. Maas, Effects of ozone addition on the kinetics and efficiencies of methane conversion at fuel-rich conditions, Appl. Energy Combust. Sci. 15 (2023) 100157.
[30] M. D'Amato, V. Magi, A. Viggiano, On iso-octane combustion with ozone addition under HCCI engine-like conditions, J. Phys.: Conf. Ser. 2385 (2022) 012086.
[31] X. Gao, Y. Zhang, S. Adusumilli, J. Seitzman, W. Sun, T. Ombrello, C. Carter, The effect of ozone addition on laminar flame speed, Combust. Flame 162 (2015) 3914–3924.
[32] T.M. Vu, S.H. Won, T. Ombrello, M.S. Cha, Stability enhancement of ozone-assisted laminar premixed Bunsen flames in nitrogen co-flow, Combust. Flame 161 (2014) 917–926.
[33] Y. Zhang, M. Zhu, Z. Zhang, R. Shang, D. Zhang, Ozone effect on the flammability limit and near-limit combustion of syngas/air flames with N2, CO2, and H2O dilutions, Fuel 186 (2016) 414–421.
[34] F. Khan, A. Elbaz, A. Katoch, J. Badra, V. Costanzo, W. Roberts, A comprehensive experimental study to measure laminar and turbulent burning velocity of Haltermann gasoline with ternary additives (O3, H2, and CO), SAE Tech. Paper (2021) 2021-01-0473.
[35] M. D'Amato, A. Viggiano, V. Magi, A numerical investigation on the laminar flame speed of methane/air and iso-octane/air mixtures with ozone addition, Combust. Flame 241 (2022) 112145.
[36] M. D'Amato, A. Cantiani, V. Magi, A. Viggiano, The laminar flame speed of iso-octane/air/ozone lean mixtures under engine-like thermo-chemical conditions, IOP Conf. Ser.: Earth Environ. Sci. (2022) 1106.
[37] H. Li, W. Liang, C.K. Law, Role of ozone addition on premixed hydrogen/oxygen flames: multi-zone structure and multi-regime dynamics, Combust. Flame 242 (2022) 112188.
[38] W. Liang, Y. Wang, C.K. Law, Role of ozone doping in the explosion limits of hydrogen-oxygen mixtures: multiplicity and catalyticity, Combust. Flame 205 (2019) 7–10.
[39] J. Crane, X. Shi, A.V. Singh, Y. Tao, H. Wang, Isolating the effect of induction length on detonation structure: hydrogen–oxygen detonation promoted by ozone, Combust. Flame 200 (2019) 44–52.
[40] W. Han, W. Liang, C. Wang, J.X. Wen, C.K. Law, Spontaneous initiation and development of hydrogen–oxygen detonation with ozone sensitization, Proc. Combust. Inst. 38 (2021) 3575–3583.
[41] H. Nishida, T. Tachibana, Homogeneous charge compression ignition of natural gas/air mixture with ozone addition, J. Propul. Power 22 (2006) 151–157.
[42] J.-B. Masurier, F. Foucher, G. Dayma, P. Dagaut, Ozone applied to the homogeneous charge compression ignition engine to control alcohol fuels combustion, Appl. Energy 160 (2015) 566–580.
[43] H. Yamada, M. Yoshii, A. Tezaki, Chemical mechanistic analysis of additive effects in homogeneous charge compression ignition of dimethyl ether, Proc. Combust. Inst. 30 (2005) 2773–2780.
[44] P.M. Pinazzi, F. Foucher, Influence of Injection Parameters, ozone seeding and residual NO on a Gasoline Compression Ignition (GCI) engine at low load, Proc. Combust. Inst. 36 (2017) 3659–3668.
[45] P.M. Pinazzi, F. Foucher, Potential of ozone to enable low load operations of a gasoline compression ignition (GCI) engine, SAE Tech. Paper (2017) 2017-01-0746.
[46] N. Seignour, A. Khacef, F. Foucher, Experimental understanding of ozone decomposition inside a low temperature combustion engine, Combust. Sci. Technol. 194 (2022) 292–303.
[47] N. Seignour, J. Masurier, B. Johansson, G. Dayma, P. Dagaut, F. Foucher, Ozone-assisted combustion of hydrogen: a comparison with isooctane, Int. J. Hydrog. Energy 44 (2019) 13953–13963.
[48] F. Anaclerio, G. Saponaro, E. Mancaruso, C. Mazzarella, F. Fornarelli, V. Magi, S. Camporeale, An experimental characterization of gasoline/ozone/air mixtures in spark ignition engines, SAE Tech. Paper (2023) 2023-24-0039.
[49] Y. Song, F. Foucher, The impact of EGR components on ozone decomposition under engine relevant conditions in a rapid compression machine, Fuel 276 (2020) 118009.

[50] S. Sayssouk, D. Nelson-Gruel, C. Caillol, P. Higelin, Y. Chamaillard, Towards control of HCCI combustion by ozone addition: a mathematical approach to estimate combustion parameters, IFAC-PapersOnLine 49 (2016) 361–8.
[51] Y. Kobashi, T.D. Dan Da, R. Inagaki, G. Shibata, H. Ogawa, Optimization of gasoline compression ignition combustion with ozone addition and two-stage direct-injection at middle loads, Int. J. Engine Res. 23 (2022) 232–242.
[52] H.A. McGee, Molecular Engineering, McGraw-Hill, New York, 1991.
[53] Ansys® Academic Research CFD, Release 20.2, ANSYS, Inc. (2020).
[54] B.F. Magnussen, On the structure of turbulence and a generalized Eddy dissipation concept for chemical reaction in turbulent flow, in: Inn Proceedings of the 19th Aerospace Sciences Meeting, St. Louis, MO, USA, 1981, 12–15 January.
[55] M. Bösenhofer, E.M. Wartha, C. Jordan, M. Harasek, The Eddy dissipation concept—analysis of different fine structure treatments for classical combustion, Energies 11 (2018) 1902.
[56] I.S. Ertesvåg, B.F. Magnussen, The Eddy dissipation turbulence energy cascade model, Combust. Sci. Technol. 159 (2007) 213–235.
[57] B.F. Magnussen, The Eddy dissipation concept—a bridge between science and technology, in: Proceedings of the ECCOMAS Thematic Conference on Computational Combustion, Lisbon, Portugal, 2005, 21–24 June.
[58] A. Parente, M.R. Malik, F. Contino, A. Cuoci, B.B. Dally, Extension of the Eddy dissipation concept for turbulence/chemistry interactions to MILD combustion, Fuel 163 (2016) 98–111.
[59] H. Bao, Development and Validation of a New Eddy Dissipation Concept (EDC) Model for MILD Combustion, Master's Thesis, Delft University of Technology, Delft, The Netherlands, 2017.
[60] M.B. Luong, Z. Luo, T.F. Lu, S.H. Chung, C.S. Yoo, Direct numerical simulations of the ignition of lean primary reference fuel/air mixtures with temperature inhomogeneities, Combust. Flame 160 (2013) 2038–2047.
[61] P. Saxena, F.A. Williams, Numerical and experimental studies of ethanol flames, Proc. Combust. Inst. 31 (2007) 1149–1156.
[62] Ansys® Academic Research CFD, Help System, Ansys Fluent Theory Guide, Release 20.2, ANSYS, Inc, 2020.
[63] Ansys® Academic Research CFD, Release 20.2, Help System, Ansys Fluent User's Guide, ANSYS, Inc, 2020.
[64] A. Viggiano, V. Magi, A comprehensive investigation on the emissions of ethanol HCCI engines, Appl. Energy 93 (2012) 277–287.
[65] F. Cramarossa, G. Dixon-Lewis, Ozone decomposition in relation to the problem of the existence of steady-state flames, Combust. Flame 16 (1971) 243–251.
[66] R. Yu, X.S. Bai, H. Lehtiniemi, S.S. Ahmed, F. Mauss, M. Richter, M. Aldén, L. Hildingsson, B. Johansson, A. Hultqvist, Effect of turbulence and initial temperature inhomogeneity on homogeneous charge compression ignition combustion, SAE Tech. Paper (2006) 2006-01-3318.
[67] A. Vressner, A. Hultqvist, B. Johansson, Study on combustion chamber geometry effects in an HCCI engine using high-speed cycle-resolved chemiluminescence imaging, SAE Tech. Paper (2007) 2007-01-0217.